# Highly efficient time-of-flight spectrometer for studying low-energy secondary emission from dielectrics: Secondary-electron emission from LiF film

S. N. Samarin[a)]
*Physics Department, University of Western Australia, Perth WA 6009, Australia*

O. M. Artamonov
*Research Institute of Physics, St. Petersburg University, St. Petersburg, Russia*

D. K. Waterhouse
*Physics Department, University of Western Australia, Perth WA 6009, Australia*

J. Kirschner and A. Morozov
*Max-Planck-Institut für Mikrostrukturphysik, Weinberg 2, D-06120 Halle, Germany*

J. F. Williams
*Physics Department, University of Western Australia, Perth WA 6009, Australia*

(Received 2 July 2002; accepted 8 November 2002)

A highly efficient time-of-flight electron spectrometer is described. An incident electron current of the order of $10^{-14}$ A makes it suitable for studying secondary emission from dielectric surfaces. A microchannel plate position-sensitive detector allows flight distance correction while keeping a large acceptance angle. Measured energy distribution curves of secondary electrons generated from a LiF film by 19–31 eV incident electrons demonstrate good energy resolution and reveal reproducible and stable emission features at $2.6\pm0.3$ eV, $7.2\pm0.3$ eV, and $10.3\pm0.3$ eV. © *2003 American Institute of Physics.* [DOI: 10.1063/1.1537044]

## I. INTRODUCTION

Emission of secondary electrons from ionic crystals (NaCl, KCl, $CaF_2$, and LiF) and films upon electron, photon, or ion impact is a very interesting and complicated phenomenon,[1–4] characterized by a high yield and relatively narrow energy distribution. This is due to the wide energy gap in their electronic structure and, by consequence, the large mean-free path of excited electrons in the solid. The possible application of these materials as highly efficient elements in electronic devices stimulated investigation of their electron emission properties. On the other hand, the decomposition of the surface, and atomic particle desorption under electron, photon, or heavy particle irradiation turns out to be related to the electron emission properties of these materials.[5,6] Although there are a number of studies of secondary-electron emission from dielectrics[1,7,8] they are almost universally hampered by charging effects and electron-stimulated modification of the surface. This is because the efficiency of conventional electrostatic analyzers used for the secondary-electron energy distribution analysis requires the incident current to be sufficiently large, usually above $10^{-9}$ A. In this article, we report the application of a highly efficient time-of-flight (TOF) electron spectrometer operating with an incident electron current of the order $10^{-14}$ A to study the energy distribution of secondary electrons from LiF films generated by 19–31 eV primary electrons. Reasonable energy resolution in the low-energy region allows identification of the emission and energy loss features in the energy distribution spectrum.

## II. TIME-OF-FLIGHT ELECTRON SPECTROMETER WITH POSITION-SENSITIVE DETECTOR

The main advantages of the TOF technique are its simplicity (the spectrometer consists basically of an electron detector) and high efficiency due to the fact that all energies are measured ''in parallel.'' The energy of the detected electron is determined by measuring its arrival time with respect to a nominated reference point on the time scale.

The principle of TOF measurement is simple.[9–11] From the measured transit time $T$ of an electron that traverses a distance $L$ in a field-free space between the sample and detector, its kinetic energy is

$$E=(m/2)(L/T)^2, \tag{1}$$

where $m$ is the electron mass. A reference point on the time scale is obtained by pulsing the incident electron beam. It follows from Eq. (1) that the relative energy resolution

$$(\Delta E/E)=[(2\Delta T/T)^2+(2\Delta L/L)^2]^{1/2} \tag{2}$$

depends on the time resolution $\Delta T$ and the uncertainty of the flight distance $\Delta L$. For straight electron trajectories and a pointlike detector (a channeltron, for example), the second term in Eq. (2) can be neglected. The time resolution $\Delta T$ is determined by the pulse width of the incident electron beam and the properties of the detector and electronics. However,

a)Electronic mail: samar@physics.uwa.edu.au

 

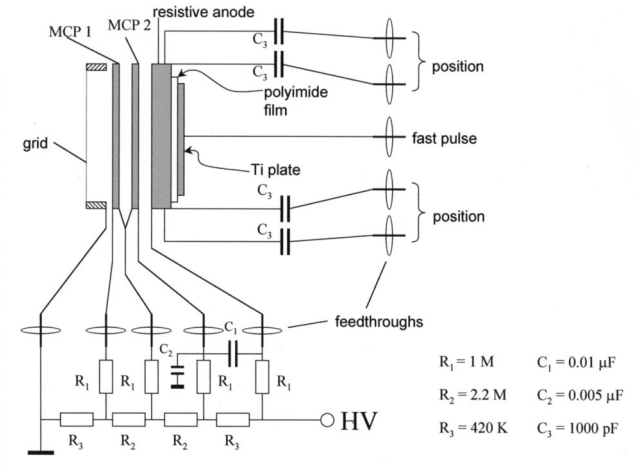


FIG. 1. Position-sensitive detector and voltage divider.

the absolute energy resolution depends as well on the electron energy to be measured and the flight distance $L$:

$$\Delta E = 2(m/2)^{-1/2} L^{-1} E^{3/2} \Delta T. \tag{3}$$

As an example, for a pulse width of 500 ps, a flight distance of 0.1 m and an electron energy of 10 eV, the energy resolution is about 0.2 eV.

The detection efficiency of the spectrometer is increased by using a large acceptance angle microchannel-plate (MCP)-based electron detector with position sensitivity (Fig. 1). Given the distance between detector and sample is 100 mm, and an active detection area 40 mm in diameter, an acceptance angle of 0.13 sr is available for electron detection. In this case, the second term in Eq. (2) is comparatively large and cannot be neglected. We describe an electron energy calculation technique that uses the position sensitivity of the detector to include a position-dependent flight time correction that takes into account the difference in flight distances for electrons arriving at the center or at the edge of the detector.

The electronic setup of the TOF spectrometer is shown in Fig. 2. An electron gun produces a pulsed electron beam with a pulse width of less than 1 ns and repetition rate of $4 \times 10^6$ Hz. The final stage of the electron gun (pulsing unit) is shown in Fig. 3. A set of input apertures selects a narrow (0.8 mm diameter) electron beam to pass between two deflection plates. Output apertures define the outgoing beam. When a negative bias of about 0.5 V is applied to the deflection plate, the electron beam is deflected out of the output

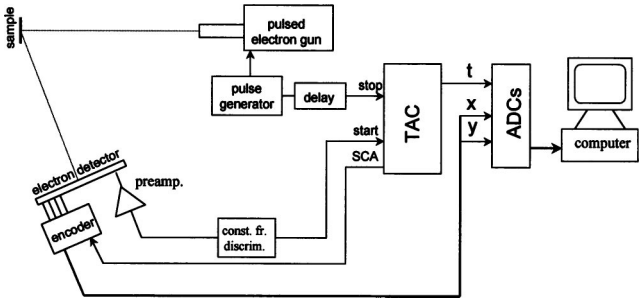


FIG. 2. Schematic diagram of the TOF spectrometer.

apertures and the sample current is zero. A short triangular-shaped positive pulse with a half width of 10 ns and amplitude of 0.5 V "opens" the gun for a short time. The real time length of the beam pulse is estimated by measuring the time distribution of elastically reflected electrons and is less than 1 ns.

The primary electrons impinge onto the sample surface and generate secondary electrons. The scattered and ejected secondary electrons from the sample are detected by an electron detector. The detector consists of two MCP's in a chevron arrangement with a resistive anode (Quantar Technology, Model 3394). A grounded grid (copper mesh, 92% transmission) is mounted in front of the first MCP, allowing the application of 200 V accelerating voltage between the grid and MCP for increased detection efficiency. A fast pulse timing signal is taken from an additional 30 mm diameter Ti plate (0.2 mm thickness) mounted behind the resistive anode. An additional insulating polyimide film was placed between the plate and resistive anode to minimize the risk of electrical breakdown.

When an electron is detected, the fast timing pulse starts a time-to-amplitude converter (TAC) and the delayed (by about 200 ns) pulse from the incident electron pulse generator stops the TAC. The TAC output amplitude is proportional to the time difference between the start and stop pulses, and is directed into an analog-to-digital converter (ADC). The time window of the TAC was chosen to be 200 ns to enable detection over a large range of electron energies, from the primary electron energy right down to below 1 eV. The low-energy limit is defined by the condition that the flight time difference between the elastically scattered electron and the electron with the lowest energy must be less than the time window (200 ns). For example, for a primary electron energy of 25 eV, the lowest energy that can be detected in a 200 ns time window is 0.8 eV. The time separation between incident electron pulses is set to 250 ns, which is 50 ns larger than the time window of TAC to decrease the probability that the slow electron "tail" generated by a previous incident pulse is detected within the present 200 ns TAC window.

The time distribution of scattered and ejected electrons from the LiF film for 28 eV primary electrons is shown in Fig. 4(a). The narrow peak in Fig. 4(a) represents elastically scattered electrons that arrive at the detector first. To make the flight distance correction mentioned earlier, the position sensitivity of the detector is utilized. For this purpose, the electron arrival position is computed by a position encoder that amplifies and processes simultaneous pulses from each of the four corners of the resistive anode. The single-channel analyzer (SCA) pulse from the TAC gates the output pulses from the position encoder. Three analogue pulses, representing the electron arrival time $T$ and $(x,y)$ position on the detector, are processed by the ADC's and stored in a list-mode file in a computer. A multiparameter acquisition system (MPA-3) (FAST ComTec) was used for data collection.

To convert the TOF to an energy for each electron trajectory, we determine the exact flight distance from the sample to the impact point on the detector and calculate $t_0$—the time when the primary electron hit the sample (and scattered electrons leave the sample). For an electron de-

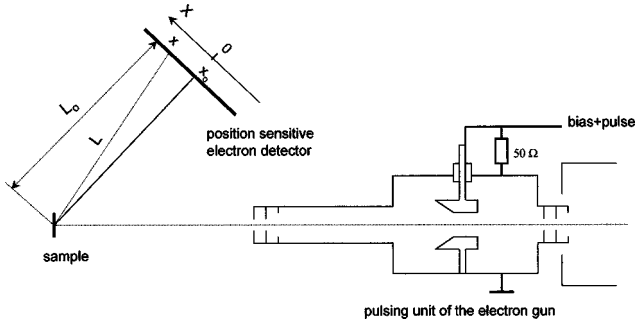


FIG. 3. Pulsing unit of the electron gun and diagram showing the different electron flight distances depending on the electron arrival position on the detector.

tected at time $T$ and at position $(x,y)$ on the detector, the flight time is $t=T-t_0$, and its flight distance is (see Fig. 3):

$$L=(L_0^2+x^2+y^2)^{1/2}. \tag{4}$$

The elastically scattered electrons, with well-defined kinetic energy $E_0$, are used to calculate $t_0$. However, the TOF of elastically scattered electrons also depends on the detection position. To reduce the position dependent spread of TOF, the measured TOF is scaled to the unique flight distance $L_0$ [see Fig. 4(a)]. In other words, the flight times are corrected so that the arrival time of each detected electron is determined as if it arrived at the center of the detector. The procedure is absolutely correct only for elastically scattered electrons with energy $E_0$, but it allows the real time spread (half width) of elastically scattered electrons to be estimated, and allows the time position $T_0$ of the elastically scattered electron maximum in the scaled spectrum to be assigned to the flight distance $L_0$. The sharp narrow maximum in the corrected TOF distribution in Fig. 4(a) denotes the arrival time $T_0$ of the elastically reflected electrons from the sample to the center of the detector. Using $T_0$, the distance $L_0$ between the sample and the detector center, and the incident electron energy $E_0$, we can calculate $t_0$ using $t_0=T_0-L_0C^{-1}E_0^{-1/2}$, where $C=(2/m)^{1/2}$.

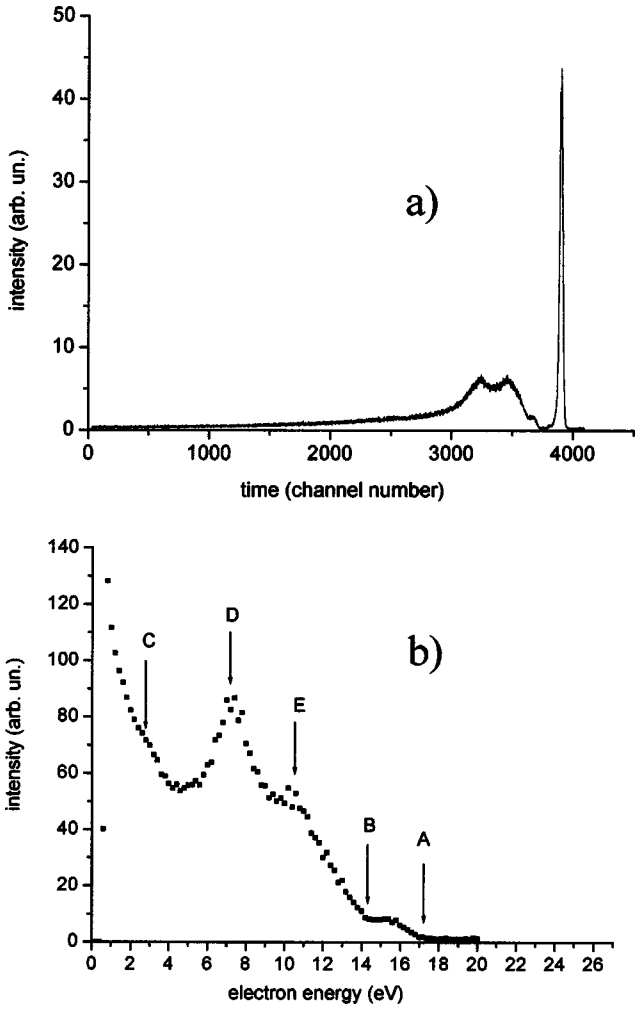


FIG. 4. TOF distribution (a) and energy distribution (b) of secondary electrons generated from LiF film by 28 eV incident electrons.

Using this information, the energy $E$ of an electron detected with coordinate $(x,y)$ on the detector at time $T$ is calculated as follows:

$$E=L^2(tC)^{-2}=(L_0^2+x^2+y^2)[(T-T_0)C+L_0E_0^{-1/2}]^{-2}. \tag{5}$$

In transforming the TOF distribution into an energy distribution and building the corresponding histogram, we also take into account the transformation of a time interval $\Delta t$ to an energy interval $\Delta E$. Figure 4(b) shows an example of the secondary-electron energy distribution obtained from the TOF distribution using the described procedure.

## III. LOW-ENERGY SECONDARY-ELECTRON EMISSION FROM LiF FILMS

To demonstrate the application of the TOF spectrometer for studying secondary emission from dielectrics, we measured energy distribution curves (EDC) of secondary electrons excited from LiF films by normal incidence low-energy primary electrons with energies from 19 to 31 eV. LiF films were evaporated on Si(100) surface from a Mo crucible heated by electron bombardment. The silicon wafer was cleaned in $NH_4OH-H_2O_2-H_2O$ (1:1:5) solution, rinsed in distilled water, and etched in HF acid. In a vacuum, it was outguessed and heated to 1200 °C until low-energy electron diffraction patterns from Si(100) surface appeared. LiF films on Si(100) surface have been studied by different techniques[12–15] and are known to be polycrystalline. Helmholz coils were used to reduce the magnetic field within the UHV chamber to less than 5 mG.

The secondary-electron energy distributions from LiF films were measured at 50° with respect to the incident electron direction using the TOF spectrometer. The EDC's are shown in Fig. 5. Measurements performed at various primary beam pulse repetition rates and different average current (in the range of $10^{-14}$ A) show no alteration in the measured spectra. This indicates that charging effects and film deterioration under the electron beam are negligible.

Five features, labeled A, B, C, D, and E, are clear in Fig. 5. The two steplike features (A and B) move on the energy scale, following the incident energy. Therefore, they represent the thresholds of characteristic energy losses at $10.3\pm0.3$ eV and $13\pm0.3$ eV, respectively. The first (A) corresponds to the exciton state in the band gap whereas the sec-

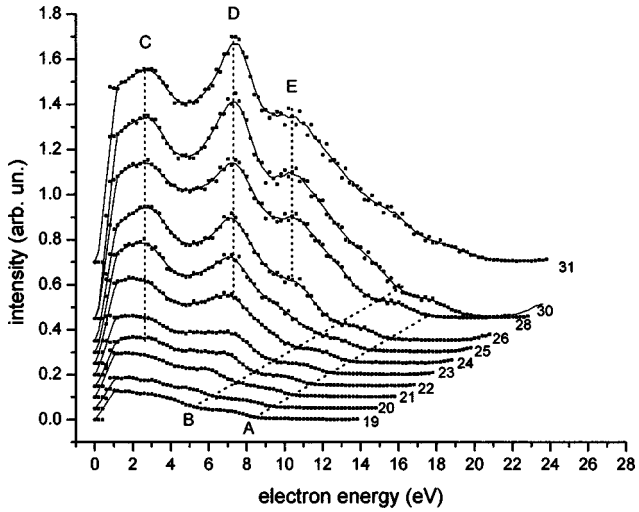


FIG. 5. EDC's of secondary electrons from LiF film. Numbers at the curves indicate incident electron energies.

ond (B) is the threshold for excitation over the band gap. This result is consistent with measurements of the electron energy loss spectrum of a LiF film with conventional electrostatic analyzers,[13,16] where broad maxima at 10.4 eV and 13.5 eV are observed.

The three maxima C, D, and E constitute emission features of the EDC's. They do not move with incident energy, but their amplitudes do change. The low-energy maximum *C* at $2.6\pm0.3$ eV starts to form at an incident energy of about 21 eV and becomes more prominent at higher primary energies. It may be due to the maximum of the unoccupied density of states at this energy.[17] A similar low-energy maximum (at $E=2.3$ eV) was observed in the EDC of soft-x-ray-induced secondary-electron emission from LiF films.[2]

The maximum D appears at a primary energy of about 24 eV. Its energy position remains constant as the incident energy increases further. A similar maximum in the EDC's of secondary electrons was observed for excitation of LiF films by photons[2] and electrons,[7,8] and was identified as being the result of plasmon decay via electron emission from the valence band. It is well established by electron energy loss spectroscopy[12,13,18] and optical measurements,[19] that bulk plasmon oscillations occur with energy $\hbar\omega_p=25\pm0.5$ eV in LiF films (and crystals). On this basis, we suggest that the maximum D at $E_D=7.2\pm0.3$ eV is due to bulk plasmon deexcitation with electron emission from the valence band. This is consistent with the energy balance: $\hbar\omega_p-E_g-\chi-\Delta E=E_D$, where $E_g$ is energy gap, $\chi$ is electron affinity, and $\Delta E$ is half width of the valence band. If $E_g=13$ eV, $\chi=0.7$ eV, and $\Delta E=4$ eV, then, $E_D=24-13-0.7-4=7.3$ eV, which is close to the observed energy of the maximum D.

When the primary energy reaches 28 eV, the next maximum in EDC, labeled E, appears at $10.3\pm0.3$ eV. The position of this maximum does not change with the primary energy. One of the reasons for this emission maximum in the EDC may be a high density of unoccupied states in this energy range as reported in Ref. 17.

## ACKNOWLEDGMENTS

The authors thank R. Muhandiramge for his help in the software design and J. Devlin, S. Key, and G. Light in the mechanical workshop in the Physics Department at UWA for technical support.

[1] F. Golek and E. Bauer, Surf. Sci. **369**, 415 (1996).
[2] B. L. Henke, J. Liesegang, and S. D. Smith, Phys. Rev. B **19**, 3004 (1979).
[3] S. Pulm, A. Hitzke, J. Gunster, H. Muller, and V. Kempter, Radiat. Eff. Defects Solids **128**, 151 (1994).
[4] F. Wiegershaus, S. Krischok, D. Ochs, W. Maus-Friedrichs, and V. Kempter, Surf. Sci. **345**, 91 (1996).
[5] L. Markowski, Surf. Sci. **501**, 235 (2002).
[6] D. Ochs, M. Brause, P. Stracke, S. Krischok, F. Wiegershaus, W. Maus-Friedrichs, V. Kempter, V. E. Puchin, and A. L. Shluger, Surf. Sci. **383**, 162 (1997).
[7] A. I. Gusarov and S. V. Murashov, Surf. Sci. **320**, 36 (1994).
[8] S. Kiyono, T. Muranaka, and A. Okazaki, Tech. Rep. Tohoku Univ. **42**, 247 (1977).
[9] Y. Uehara, T. Ushiroku, S. Ushioda, and Y. Murata, Jpn. J. Appl. Phys., Part 1 **29**, 2858 (1990).
[10] O. Hemmers, S. B. Whitfield, P. Glans, H. Wang, and D. W. Lindle, Rev. Sci. Instrum. **69**, 3809 (1998).
[11] R. Z. Bachrach, F. C. Brown, and S. B. M. Hagström, J. Vac. Sci. Technol. **12**, 309 (1975).
[12] F. Golek and W. J. Sobolewski, Solid State Commun. **110**, 143 (1999).
[13] F. Golek and W. J. Sobolewski, Phys. Status Solidi **210**, R1 (1998).
[14] D. A. Lapiano-Smith, E. A. Ekund, F. J. Himpsel, and L. J. Terminello, Appl. Phys. Lett. **59**, 2174 (1991).
[15] H. Guo, H. Kawanowa, and R. Souda, Appl. Surf. Sci. **158**, 159 (2000).
[16] G. Roy, G. Singh, and T. E. Gallon, Surf. Sci. **152**, 1042 (1985).
[17] A. B. Kunz, T. Miyakawa, and S. Oyama, Phys. Status Solidi **34**, 581 (1969).
[18] C. Gout and F. Pradal, J. Phys. Chem. Solids **29**, 581 (1968).
[19] M. Greuzburg, Z. Phys. **196**, 433 (1996).